PASJ: Publ. Astron. Soc. Japan **59**, S815–S821, 2007 November 30

Diagnostics of Radio Fine Structures around 3 GHz with Hinode Data in the Impulsive Phase of an X3.4/4B Flare Event on 2006 December 13

Yihua YAN, Jing HUANG, and Bin CHEN
National Astronomical Observatories, Chinese Academy of Sciences, Beijing 100012, China
yyh@bao.ac.cn, huangjing04@bao.ac.cn, chenbin@bao.ac.cn
and
Takashi SAKURAI
National Astronomical Observatory of Japan, 2-21-1 Osawa, Mitaka, Tokyo 181-8588
sakurai@solar.mtk.nao.ac.jp

(Received 2007 May 31; accepted 2007 September 11)

Abstract

On 2006 December 13 during the solar minimum, the superactive region NOAA 10930 at the S05W33 disk location produced an X3.4/4B flare at 02:40 UT. Fine structures were observed in the radio spectra, which included spikes, reverse slope-type III bursts, type-U burst, V-shaped burst, pulsations, zebra patterns, and firstly discovered sub-second spiky zebra-like structures, superimposed on the 2.6–3.8 GHz type IV bursts. The radio fine structures during the impulsive phase of the flare may be closely associated with coronal structures during the magnetic-reconnection process, as revealed by Hinode soft X-ray images. Thus, these microwave fine structure observations may provide very useful diagnostics at the primary energy release sites when they occur in the impulsive flare phase. For this flare event, the estimated coronal magnetic field is about 50–170 G in the rising phase of the flare with a source density of about 1×10^{11} cm^{-3}. The field strength and plasma density are about 90–200 G and 1.27×10^{11} cm^{-3} around the flare maximum.

Key words: coronal magnetic field — radio fine structures — solar flares — solar radio bursts — Sun: radio emission

1. Introduction

Radio emission in the solar corona is generated by thermal and nonthermal (up to highly-relativistic) electrons, and thus provides important diagnostics complementary to EUV, soft X-rays (SXR), hard X-rays (HXR), and γ-rays (Aschwanden 2004). In particular, the frequency range from a few hundred MHz to several GHz corresponds to source densities of a few 10^8 to 10^{11} cm^{-3}, which is the range of densities where primary energy release of flares is expected to take place (Bastian et al. 1998; Benz 2004). The radio fine structures, such as spikes, zebra patterns, pulsations, are generally considered to be closely related to the primary energy release processes if they occur in the impulsive flare phase (Zaitsev & Stepanov 1983; Bastian et al. 1998; Zlotnik et al. 2003; Aschwanden 2004; Benz 2004; Chernov 2006). The stripes of the zebra patterns in the microwave range with separate spike-like pulses of millisecond duration (< 8 ms) are related to magnetic reconnection above flaring regions by either the whistler wave model (Chernov et al. 2003) or the mechanism of double plasma resonance (DPR: Kuznetsov & Tsap 2007). In the latter case, the periodic injection of electron beams into the coronal arcade may cause pulsed spikes in the zebra stripes. On 2006 December 13 during the solar minimum, the superactive region NOAA 10930 at S05W33 disk location produced an X3.4/4B flare at 02:40 UT. Complicated radio bursts with a 44000 SFU at 10 cm wavelength, a type II burst with a shock speed of 1534 km s^{-1}, and type IV radio sweeps were associated with this event, as well as a fast-moving CME with an estimated projected speed of 1500 km s^{-1}, according to the Solar Geophysical Data (SGD) web data. A γ-ray burst was also reported for this event (SGD). Very rich complicated radio fine structures were observed during a long period from 02:20 to 05:10 UT by the spectropolarimeters at the Huairou Station of the National Astronomical Observatories of China (Huairou/NAOC) with very high temporal (5–8 ms) and spectral (10–20 MHz) resolutions in 2.6–3.8 GHz and 5.2–7.6 GHz ranges (Fu et al. 2004). Hinode (Kosugi et al. 2007), RHESSI (Lin et al. 2002), and other satellites recorded rich EUV, soft X-ray (SXR), and hard X-ray (HXR) data for this event. It therefore provides us a good opportunity to perform plasma and magnetic field diagnostics in the source region for this X3.4/4B event. Here we concentrate on the occurrence of radio fine structures superimposed in the microwave-type IV bursts during the rising process of the flare and its associations with coronal structures, as revealed by Hinode observations (at this time interval there are no any other high cadence imaging data available). In the next section, we introduce observations and data analysis. Then in section 3 we discuss the inferred source plasma and magnetic field parameters for this flare event, and draw our conclusions.

2. Observations and Data Analysis

Magnetic field measurements were obtained from SOHO/MDI (Scherrer et al. 1995), and the HXR observations were obtained with RHESSI (Lin et al. 2002). The SXR images were obtained with the X-Ray Telescope (XRT) aboard

Table 1. Observed parameters of some zebra patterns.

Zebra event (UT)	Duration (s)	Frequency range f (GHz)	Frequency separation Δf (MHz)	Number of stripes Δs	Relative bandwidth $\Delta f/f$	Polarization
02:22:29	~ 7	< 2.60–2.95	40–60	4–7	0.015–0.021	full RHCP
02:23:02	> 2	< 2.60–3.15	20–40	> 14	0.007–0.014	full RHCP
02:23:35	~ 4	< 2.60–3.17	40–70	> 8	0.014–0.024	full RHCP
02:24:04	0.22	2.89–3.03	50	4	0.017	full RHCP
02:24:05	0.2	2.87–2.98	40	3	0.014	full RHCP
02:42:58	42	2.60–3.80	80–180	8	0.025–0.056	strong RHCP

Hinode (Golub et al. 2007). The spectrum data of radio bursts were obtained by the Huairou/NAOC spectrometers in the frequency ranges of 2.6–3.8 GHz and 5.2–7.6 GHz (Fu et al. 2004) with a data-processing method introduced in Yan et al. (2002). Figure 1 shows the temporal profiles of SXR, HXR, and radio bursts at 2.84 GHz and 5.7 GHz, and the dynamic spectra of right-handed circular polarization (RHCP) in 2.6–3.8 GHz and 5.2–5.8 GHz (only the lower-frequency part of the 5.2–7.6 GHz Huairou/NAOC spectrometer was operating) from 02:00 UT to 05:10 UT on 2006 December 13. A rich variety of radio fine structures, including spikes, zebra patterns, and spiky zebra features (with various durations down to < 0.1 s), narrow type III bursts, pulsations and drifting pulsation structures, fibers, mixed fast and slow drifting stripes, etc., were recorded. During the rising phase of the flare, mainly RHCP components of numerous fine structures were observed to be superimposed on the microwave type IV bursts. Here, we are interested in the time interval 02:21–02:25 UT, as indicated in figure 1, because first groups of many fine structures appeared, and they corresponded to the coronal topological changes, as revealed by Hinode SXR images. Before the rapid increase of the flare emission, an enhancement of radio bursts accompanied some weak fine structures, such as microwave type III bursts during 02:21–02:22 UT with reverse frequency drift rates ranging from $\sim 1\,\mathrm{GHz\,s^{-1}}$ to $3.6\,\mathrm{GHz\,s^{-1}}$ in the 2.6–3.8 GHz range. A subsecond type U burst occurred at 02:21:45 UT with $-1.7\,\mathrm{GHz\,s^{-1}}$ normal and $1\,\mathrm{GHz\,s^{-1}}$ reverse drifts at a turning frequency of 2.7 GHz. A V-shaped burst occurred at 02:21:54 UT, which may correspond to the reflection of electron beams with $0.8\,\mathrm{GHz\,s^{-1}}$ to $-1.25\,\mathrm{GHz\,s^{-1}}$ drift rates. Then, during 02:22:30–02:22:34 UT the first zebra pattern for this flare event occurred, accompanied by spikes, pulsations, reverse type III, and diffuse continuum bursts, as shown in figure 2a. During 02:22:57–02:23:04 UT, about 14 parallel stripes were mixed with dense pulsations of about 40–50 ms separation intervals and ending at intense type-III bursts with a reverse-drifting slope of about $1.1\,\mathrm{GHz\,s^{-1}}$, as shown in figure 2b. Figure 2c shows another zebra pattern and strong pulsations occurred during this period. The pulsations extended to 3.8 GHz before a group of spikes appeared at 02:23:35 UT in the frequency range up to 3.4 GHz for the duration of less than 1 s. Zig-zag parallel stripes were observed at the same time, lasting for about 4 s. For each vertical pulsation structure, the intensity along its lower part section, which overlaps the frequency band of the zebra patterns, seems to become weak, but may become bright again when downward bursts occurred, e.g., a confined continuum enhancement appeared after 02:23:38 UT as shown in figure 2c. After 02:23:25 UT for nearly one minute duration, enhanced continuum emission occurred with a bright RHCP continuum in the frequency range from less than 2.6 GHz (due to our band limit) to a higher cutoff frequency of up to about 2.9 GHz. Around this continuum with extensions to higher frequency, many short-period fine structures including spikes, narrow band pulsations, type III bursts, zebras, fibers, and spiky sub-second zebra-like features were observed before a broad band continuum enhancement from about 02:25 UT. More than 50 individual fine structures during 02:22 – 02:25 UT could be registered, and two such spiky sub-second zebra-like super-fine structures are shown in figure 2d. The observed features of the above-discussed zebra patterns as well as one strong RHCP zebra pattern at 02:42–02:43 UT, two minutes after the flare maximum shown in figures 2e–2f, are summarized in table 1. Discussions concerning the spikes and pulsations as well as their associations with the 2006 December 13 flare event are presented elsewhere (e.g., Tan et al. 2007). The RHESSI HXR telescope did not cover this period due to satellite night (figure 1). In figure 3, the MDI magnetogram of the NOAA 10930 region shows the main negative leading sunspot and positive following sunspots, whereas high cadence Hinode/XRT SXR images from 02:21 UT to 02:25 UT show that the coronal structures above NOAA 10930 underwent a topological change from an east–west rope-like structure to a north–south arcade structure with an expansion in the north–south direction. The SXR brightening started at 02:22:18 UT and reached its maximum at 02:24:18 UT with explosive features (the images were saturated at bright patches). Then, the SXR flaring areas shrank at 02:25:18 UT to cover a confined area of the twisting loop or arcade structure. The SXR coronal structure continued to develop into more or less north–south aligned loops or the post-flare arcade structure with expansion in the north–south direction. The Hinode SXR images during 02:41–02:45 UT corresponding to the zebra pattern burst shown in figures 2e–2f are demonstrated in the bottom panels of figure 3. A detailed analysis of the evolution of the flaring loop systems in the early phase of the flare towards the onset of the impulsive phase can be found in T. Sakao et al. (2007, presentation at the Initial Result from Hinode Workshop). The flare ribbons evolved in an anticlockwise way from an east–west separation during the impulsive phase to a north–south separation in the post-flare phase, with ribbon footpoints expanding more

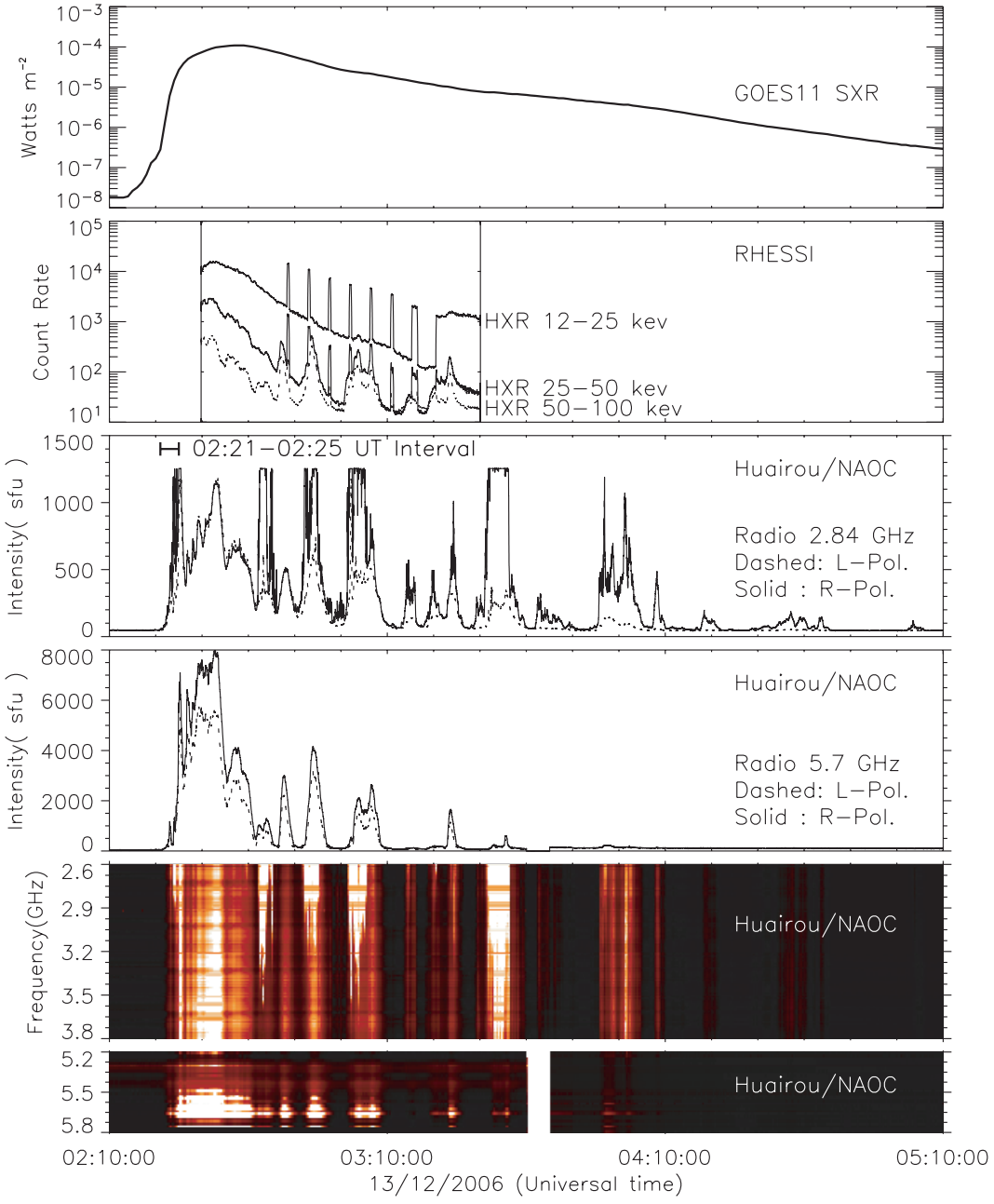

Fig. 1. Temporal profiles of GOES SXR, RHESSI HXR, and radio fluxes at 2.84 GHz and 5.7 GHz, and the dynamic spectra of the RHCP component in 2.6–3.8 GHz (bright/dark: 1000/100 SFU) and 5.2–5.8 GHz (bright/dark: 2000/100 SFU) from 02:10 UT to 05:10 UT on 2006 December 13. The RHCP time profile at 2.84 GHz was saturated when strong bursts occurred. The blank area in the 5.2–5.8 GHz dynamic spectrum image was due to a data gap.

closely to the sunspot centers. From MDI magnetogram data, the line-of-sight magnetic fields corresponding to the ribbon footpoints increased from 800 G to 1300 G. We note that the above-mentioned radio fine structures (as shown in figures 2a–2d) occurred just during the rising phase when the topological change of coronal SXR structures took place from a rope-like structure to an arcade structure in 02:21–02:25 UT, whereas the broadband bursts including a zebra pattern that occurred about 2 min after the flare peak shown in figures 2e–2f may correspond to the post-flare process.

3. Discussion and Conclusion

As mentioned above, the microwave zebra patterns with separate spike-like pulses of millisecond duration are interpreted as being due to magnetic reconnection above flaring regions by either the whistler wave model (Chernov et al. 2003) or the DPR mechanism (Kuznetsov & Tsap 2007). In the DPR model, the periodic injection of electron beams into coronal arcade may cause the pulsed spikes in the zebra stripes. Both pulsations and the zebra pattern could be caused by the repeated injection of non-thermal electrons. The

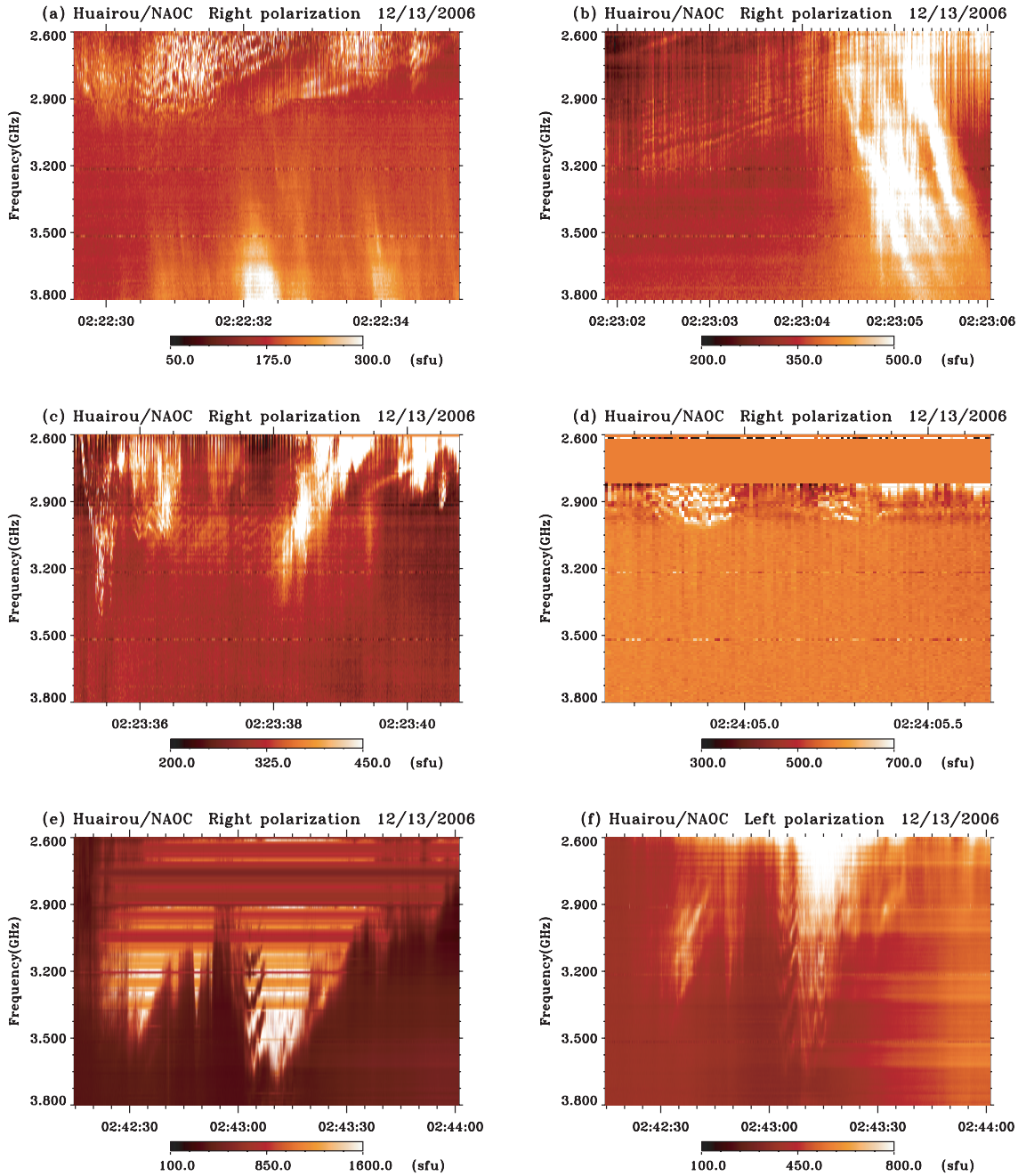

Fig. 2. Dynamic spectra of some full and strong RHCP fine structures: (a) first spiky zebra pattern structure occurring during 02:22:30–02:22:35 UT; (b) second zebra pattern structure mixed with pulsations and bright reverse drifting type III bursts during 02:23:02–02:23:06 UT; (c) spikes, zebra pattern structure, pulsations, and type IV continuum emission during 02:23:35–02:23:40 UT; (d) two sub-second spiky zebra patterns with about 0.2 s duration at 02:24:05 UT extending to higher frequencies from the type IV continuum emission; the RHCP (e) and LHCP (f) dynamic spectra during 02:42–2:44 UT including a zebra pattern structure. The horizontal shadows in (d–e) were due to saturation of the RHCP component.

downward electron beams lead to the periodic pulsations, and while they reach the emission region of zebra stripes, the particle momentum distribution could be altered by capture or scattering processes. Generally, different particle distributions over momentum can result in different intensities of zebra stripes versus background. For example, in the DPR model, a power-law distribution, which is typical for electron beams, can generate more powerful zebra stripes than Maxwellian distribution (see, e.g., Kuznetsov & Tsap 2007), which may correspond to the case of figure 2c. During the time intervals as described above for the 2006 December 13 flare event, the Hinode SXR images demonstrated bright features which may correspond to the region below a magnetic reconnection site where the radio sources of zebra patterns could probably be located. It is suggested from these data that the radio source is at a height of about 15–20 Mm. We may also estimate the coronal magnetic field and the electron density at the source volume from the zebra and the spiky zebra-like features

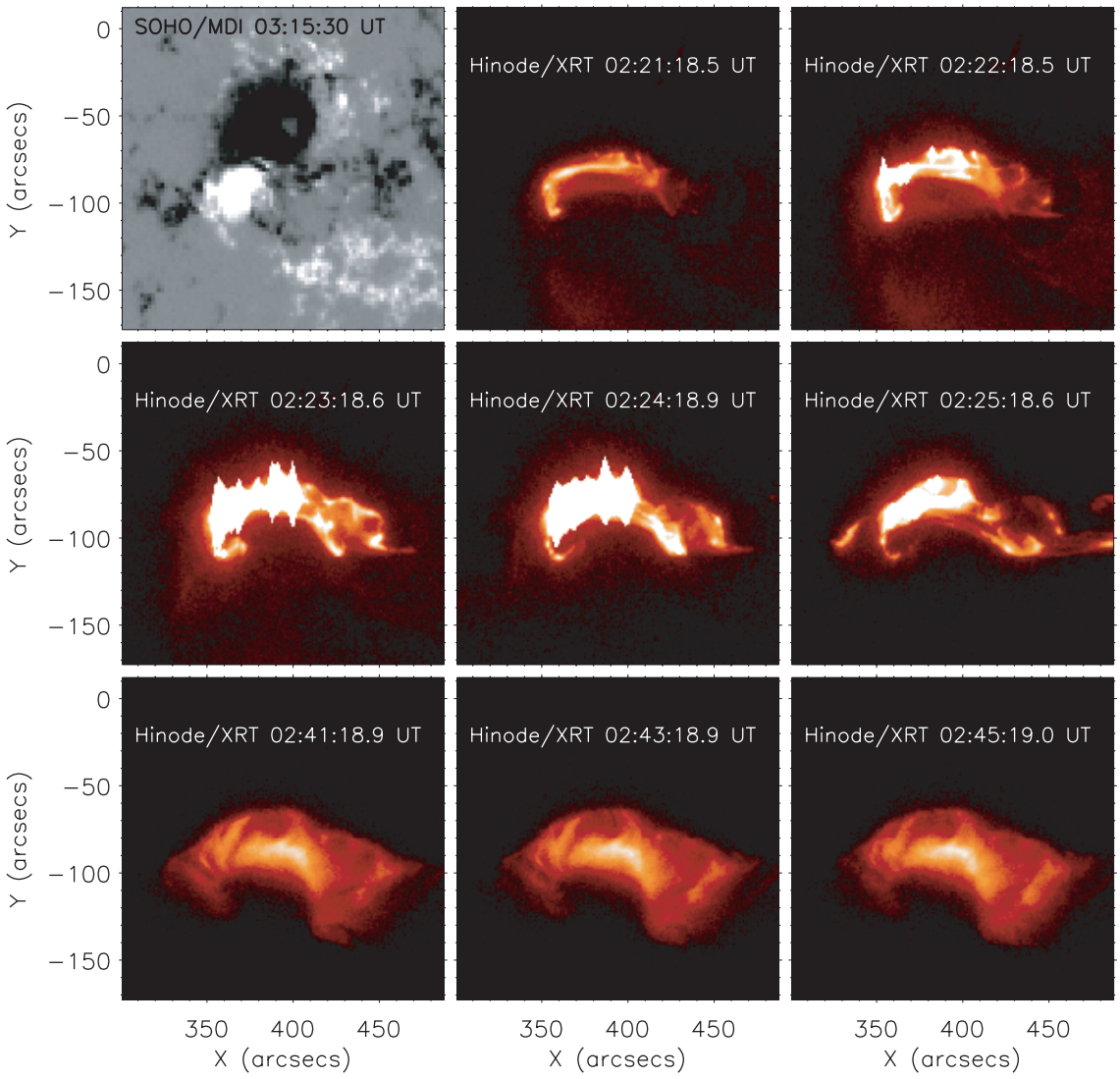

Fig. 3. SOHO/MDI magnetogram for NOAA 10930 at 03:15:30 UT (white/black: ±400 G) and Hinode SXR images from 02:21 to 02:25 UT, showing the impulsive phase and from 02:41 to 02:45 UT, showing the post-flare arcade. Note there were saturations at bright patches for the impulsive phase SXR images.

(listed in table 1) by both the whistler wave model (Chernov et al. 2003) and the double plasma resonance model (Kuznetsov & Tsap 2007). From whistler wave model (Chernov 2006), it is assumed that

$$\Delta f_{\rm ea} \approx f_{\rm w} \approx 0.1 f_B, \tag{1}$$

where $\Delta f_{\rm ea}$ is the frequency separation between a stripe emission and its adjacent low-frequency absorption, $f_{\rm w}$ is the frequency of a whistler wave, and $f_B = \dfrac{eB}{2\pi m_{\rm e} c} = 2.8\,B$ (MHz) is the electron gyrofrequency, where e and $m_{\rm e}$ are the electron charge and mass, respectively, c is speed of light, and B is in G. In the case that an absorption signature is not significant, the value of $\Delta f_{\rm ea}$ is assumed to be half of Δf. Therefore, the magnetic field can be estimated from equation (1) by the whistler wave model. From the DPR model (Kuznetsov & Tsap 2007), the frequency separation, Δf, is related to the harmonic frequencies, f_s, by

$$\frac{\Delta f}{f} = \frac{f_{s+1} - f_s}{f_s} \approx \frac{f_{\rm p}(h_{s+1}) - f_{\rm p}(h_s)}{f_{\rm p}(h_s)} \approx \frac{1}{s}\frac{1}{1-(2L_n/L_B)}, \tag{2}$$

where s is the harmonic number, $f_{\rm p}$ is the plasma frequency, h_s is the height of s harmonic resonant layer, L_n and L_B are the characteristic scale heights of plasma density $n_{\rm e}$ and magnetic field, respectively, which are determined by

$$L_n = n_{\rm e}\left(\frac{\partial n_{\rm e}}{\partial h}\right)^{-1}, \quad L_B = f_B\left(\frac{\partial f_B}{\partial h}\right)^{-1}. \tag{3}$$

Assuming $\Delta s = s_2 - s_1$ (note that low harmonic number corresponds to high frequency when $L_B < 2L_n$) and denoting $\delta = \Delta f / f$, one has

$$s_1 \approx \frac{\Delta s \delta_2}{\delta_1 - \delta_2}, \quad \frac{L_n}{L_B} \approx \frac{1}{2}\left(1 + \frac{1}{\delta_1 s_1}\right). \tag{4}$$

From the observed data, the plasma density and the magnetic

Table 2. Estimated magnetic field intensity and plasma density in the source region.

Zebra event (UT)	By whistler wave model (G)	By DPR model (G)	Scale height ratio (L_n/L_B)	Source density (10^{11} cm^{-3})
02:22:29	71.4–107.1	97.1–145.7	3.90	0.92
02:23:02	35.7– 71.4	48.6– 97.1	3.9*	1.03
02:23:35	71.4–125	97.7–171.0	3.92	1.06
02:24:04	89.3	121.4	3.9*	1.09
02:24:05	71.4	97.1	3.9*	1.06
02:42:58	142.8–321.3	90.9–204.4	2.09	1.27

* The characteristic scale height ratio L_n/L_B is assumed to be 3.9.

field can be estimated by the DPR model. The results by both methods are summarized in table 2. It can be seen that qualitatively the magnetic fields derived from both methods agree with each other. The estimated source density is around 10^{11} cm^{-3}. We also found from the DPR model that the value of L_n/L_B, which is properly derived from observed data in the impulsive phase around 02:23 UT, is 3.9, about 2-times that value of 2.09 after the flare maximum at 02:43 UT. If we consider that the density scale height does not change significantly, the magnetic field scale height would increase by a factor of 2 from the impulsive phase of the flare to its maximum, or the magnetic field versus altitude in the impulsive phase would be less varying than around the flare maximum by a factor of 2. This should be a reasonable result as two-ribbon flares develop. The magnetic field derived from the DPR model is $\sim$50–170 G in the source regions during the impulsive phase, and increases to $\sim$90–200 G at 02:42 UT around the flare maximum. We may also estimate the magnetic field value at 15–20 Mm height, which should be the radio source locations from the empirical formula (Dulk & McLean 1978),

$$B = 0.5(R/R_\odot - 1)^{-1.5} \quad (1.02 \lesssim R/R_\odot \lesssim 10), \tag{5}$$

which gives a value of 47–60 G. However, the field value at the chromosphere with $R = 1.02R_\odot$ is only 176 G by the above formula, whereas the photospheric field values at ribbon footpoints are around 800 G to 1300 G from 02:23 UT to 02:43 UT, which would produce much greater field values at the chromosphere. If we consider that the above formula is valid for the observed data by a factor of three (Dulk & McLean 1978), we would obtain 140–177 G at 15–20 Mm altitude, which is consistent with the above model estimations. Since the flare ribbon separation with time was firstly east–western-ward, and then in an anticlockwise way to north–southern-ward direction, the corresponding footpoint fields would increase as the ribbons approach the sunspot centers. This is consistent with the rising field results with time, as given in table 2. In summary, the fine structures including newly discovered sub-second spiky zebra patterns superimposed in the microwave type IV bursts during the impulsive phase of the flare are closely associated with coronal structures during magnetic reconnection process as revealed by Hinode SXR images. Therefore, these radio observations should be closely related to the primary energy release site, and may provide very useful diagnostics in the source region. For the 2006 December 13 X3.4/4B flare event, the derived magnetic field scale height would increase by a factor of two from the impulsive phase at 02:23 UT to around the flare maximum at 02:43 UT, if the source density scale height is assumed to not change significantly. The estimated coronal field is about 50–170 G in the rising phase of the flare with a source density of about 1×10^{11} cm^{-3}. The field value and the plasma density are about 90–200 G and 1.27×10^{11} cm^{-3} around the flare maximum.

This work is supported by the National Basic Research Program of the MOST (Grant No. 2006CB806301) and CAS-NSFC Key Project (Grant No. 10778605). Hinode is a Japanese mission developed and launched by ISAS/JAXA, with NAOJ as a domestic partner and NASA and STFC (UK) as international partners. It is operated by these agencies in co-operation with ESA and NSC (Norway). The participation of National Astronomical Observatories of China in the analysis of Hinode data is based on a Letter of Agreement signed in 2006 July with ISAS/JAXA and NAOJ. We thank particularly the XRT team for the data used in figure 3. We are also grateful to the availability of SOHO/MDI, RHESSI, and GOES online data.

References

Aschwanden, M. J. 2004, Physics of the Solar Corona (Berlin: Springer-Verlag), Chap.15
Bastian T. S., Benz A. O., & Gary D. E. 1998, ARA&A, 36, 131
Benz, A. O. 2004, in Solar and Space Weather Radiophysics, ed D. E. Gary & C. O. Keller (Dordrecht: Kluwer), 203
Chernov, G. P. 2006, Space Sci. Rev., 127, 195
Chernov, G. P., Yan, Y. H., & Fu, Q. J. 2003, A&A, 406, 1071
Dulk, G. A., & McLean, D. J. 1978, Sol. Phys., 57, 279
Fu, Q., et al. 2004, Sol. Phys., 222, 167
Golub, L., et al. 2007, Sol. Phys., 243, 63
Kosugi, T., et al. 2007, Sol. Phys., 243, 3
Kuznetsov, A. A., & Tsap, Y. T. 2007, Sol. Phys., 241, 127
Lin, R. P., et al. 2002, Sol. Phys., 210, 3
Scherrer, P. H., et al. 1995, Sol. Phys., 162, 129
Tan, B., Yan, Y., Tan, C., & Liu, Y. 2007, ApJ in press
Yan, Y., Tan, C., Xu, L., Ji, H., Fu, Q., & Song, G. 2002, Sci. China, Ser. A, 45, 89
Zaitsev, V. V., & Stepanov, A. V. 1983, Sol. Phys., 88, 297
Zlotnik, E. Y., Zaitsev, V. V., Aurass, H., Mann, G., & Hofmann, A. 2003, A&A, 410, 1011